Controlling substrate temperature with infrared heating to improve mechanical properties of large-scale printed parts*

Andrzej Nycz[1], Vidya Kishore[1], John Lindahl[1], Chad Duty[1,2], Charles Carnal[1], Vlastimil Kunc[1,2,3]

[1]Manufacturing Demonstration Facility, Oak Ridge National Laboratory
[2]University of Tennessee, Knoxville
[3]Purdue University

Abstract

Additively manufactured parts made with polymer extrusion techniques can be 50-75% weaker in the z-direction (across layers) than in the x- and y-directions. This has been attributed to poor mobility of polymer chains and a low degree of entanglement across a cold deposition interface. This is particularly a challenge when printing large-scale parts, such as with the Big Area Additive Manufacturing (BAAM) system, because layer times can exceed several minutes. The current work presents a method for controlling the temperature of the substrate material on the BAAM just prior to deposition using infrared heating lamps. Long layer times were also simulated by actively cooling the material following deposition of each layer. The effect of substrate temperature on the z-direction mechanical properties of 20% carbon fiber reinforced acrylonitrile butadiene styrene (ABS) was measured for an initial temperature ranging from 50 °C to 150 °C and a preheated temperature ranging from 150 °C to 220 °C. Infrared preheating proved to be very effective when applied to substrates that had cooled considerably, almost doubling the tensile strength and increasing the fracture toughness by a factor of 7x.

Background

Large format additive manufacturing (AM) for extrusion-based polymers has become increasingly popular since the development of the Big Area Additive Manufacturing (BAAM) system [1, 2]. The current version of the BAAM system has a build volume that measures 6 m x 2.5 m x 1.8 m and is capable of depositing material at a rate of up to 50 kg/h. BAAM uses a pelletized thermoplastic feedstock that is common to injection molding and traditional extrusion industries. The material grades can range from common acrylonitrile butadiene styrene (ABS) to high performance semi-crystalline polymers such as polyphenylenesulfide (PPS) [3, 4]. Large format deposition systems often utilize materials reinforced with chopped carbon fibers in order to provide additional stiffness in the component and to reduce thermally-induced distortion [5]. The large format deposition system has been demonstrated by such notable projects as printed

automobiles [6, 7], a submersible vehicle [8], a house [9], and a world record-setting trim tool for aerospace applications [10].

One of the challenges associated with 3D printed components is the natural anisotropy of mechanical properties due to the layer-wise deposition process. 3D printing conventionally occurs by depositing material in a plane (x-y) that is parallel to the build plate and sequentially adding layers of material in the z-direction. Since the deposited material is continuous in the x-y plane, but only bonded at discrete areas between the layers, the strength in the x- and y-directions is often significantly greater than along the z-axis. For instance, Ahn conducted tensile tests on ABS samples printed on a small-scale printer in various orientations and found the x-axis strength to be 6-7 times greater than the corresponding strength along the z-axis [11]. Shaffer likewise demonstrated an orientation dependence of 6x for ABS and almost 2x for polylactic acid [12]. Torrado-Perez also showed a 2x reduction in strength for ABS small-scale samples (28.4 MPa vs 14.1 MPa) [13]. Duty conducted mechanical tests on BAAM-printed samples, showing a slight orientation dependence for unreinforced ABS, but a much more significant effect (~8x) for 20% carbon fiber reinforced ABS [14]. Such a drastic difference in the directional mechanical strength of printed components indicates a poor bond between successive layers, especially for large components.

There have been a number of efforts to reduce the mechanical anisotropy of printed components, either during the printing process or as a post-deposition step. Shaffer found that by exposing printed components to ionizing radiation, a crosslinking reaction between layers of PLA was initiated that reduced anisotropy by 20-50% [12]. Sweeney was able to improve the bond strength of printed components by 275% by using localized microwave heating of polymer composites containing carbon nanotubes [15]. Duty found that by depositing material into intentionally aligned voids in the z-direction of a printed part, the z-strength could be increased by 250% for fiber reinforced PLA [16].

As the size of printed components increases, the deposition time required for a given layer increases as well – causing the underlying material to cool considerably before the next layer is deposited [17]. The thermal history of the interface between the freshly deposited material and the previous layer can have a significant impact on the integrity of the bond that is formed between layers. Sun proposed that the interfacial temperature needed to stay above the glass transition temperature (T_g) of the material in order to allow for interfusion of the molecular chains [18]. Turner used a Newtonian sintering model and found that very little neck formation (or molecular bonding) occurs below a critical temperature, which was found to be well above the T_g for ABS (200 °C vs 94 °C) [19]. Turner proposed that a significant degree of molecular chain motion occurs between the T_g and the critical temperature identified by the neck formation model. Partain attempted to elevate this bonding temperature during deposition by actively heating the interface with forced air [20]. However, the heated jet disturbed the deposition geometry too much to produce improved strength. Ravi used a laser-based system to increase the bonding interface and demonstrated a 50% increase in flexural strength [21, 22].

The current study builds on previous work by the authors [23-25] to control the interfacial temperature during the printing process by using infrared radiation to preheat the surface of a printed layers just prior to deposition of the next layer. Our previous study found that the average fracture energy of samples that were preheated could be increased by 200% over the unheated samples.

The current study refines the experimental set-up and print conditions to enable better control of the substrate temperature before and after preheating and to better understand the effects of preheating. The previous efforts primarily used variations in print speed, intensity of the lamps (heat input), and extrusion temperature to modify the substrate temperature before and after preheating. There was no active control of substrate temperature, so the previous study had several cases of excessive heating which likely degraded the polymer at the interface, thereby weakening the material in the z-direction. In the current work, the substrate temperature during preheating was actively controlled. Print speed and deposition temperature were held constant and the substrate temperature was controlled with artificial cooling and infrared lamps. This approach reduced overheating issues and provided a way to adjust the substrate temperature to ranges well below T_g.

Experimental Method

A symmetric hexagon structure, shown in Figure 1, was deposited on an experimental Blue Gantry (BG) system at the Manufacturing Demonstration Facility (MDF). The BG system is functionally similar to a BAAM printer with a working envelope of 2.0 m x 2.0 m x 1.3 m. The BG system has an open configuration that is ideal for experiments which require hardware attachments and signal cabling in close proximity to a part during printing. The system also features an automatic feed system capable of continuously delivering polymer pellets for build times in excess of 20 hours. The material used for this study was carbon fiber reinforced ABS (J-1200/CF/20 3DP supplied by Techmer PM) with a T_g of 105 ^oC. An in-house slicer software [26] produced G-code from STL files of the hexagons, which measured 1.2 m long x 0.6 m wide x 0.3 m tall. A cross section of the hexagon wall consisted of a stack of 67 single beads measuring approximately 9 mm in width and an individual layer height of 3.8 mm. The beads were extruded through a 7.6 mm diameter nozzle and were compressed to a width of 9 mm with a tamping mechanism [14] shown at the end of the print head in Figure 2. The print speed for the hexagons was held constant at 5 cm/s, the base was heated to a temperature of 93 °C, and the deposition temperature was 230 ^oC.

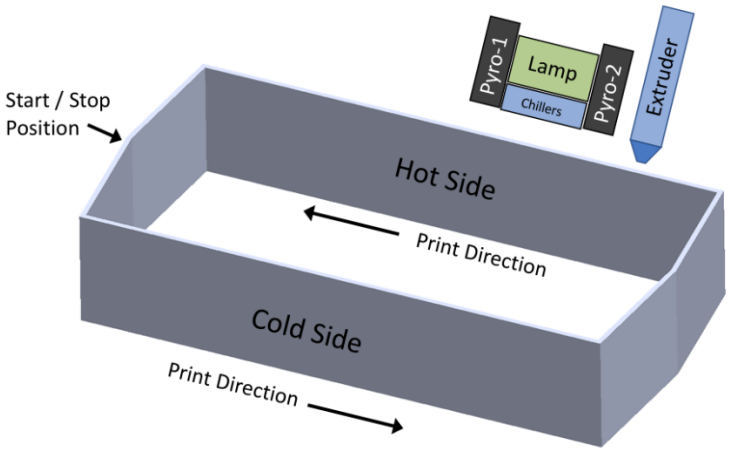

Figure 1. Hexagon structure for IR preheating experiments.

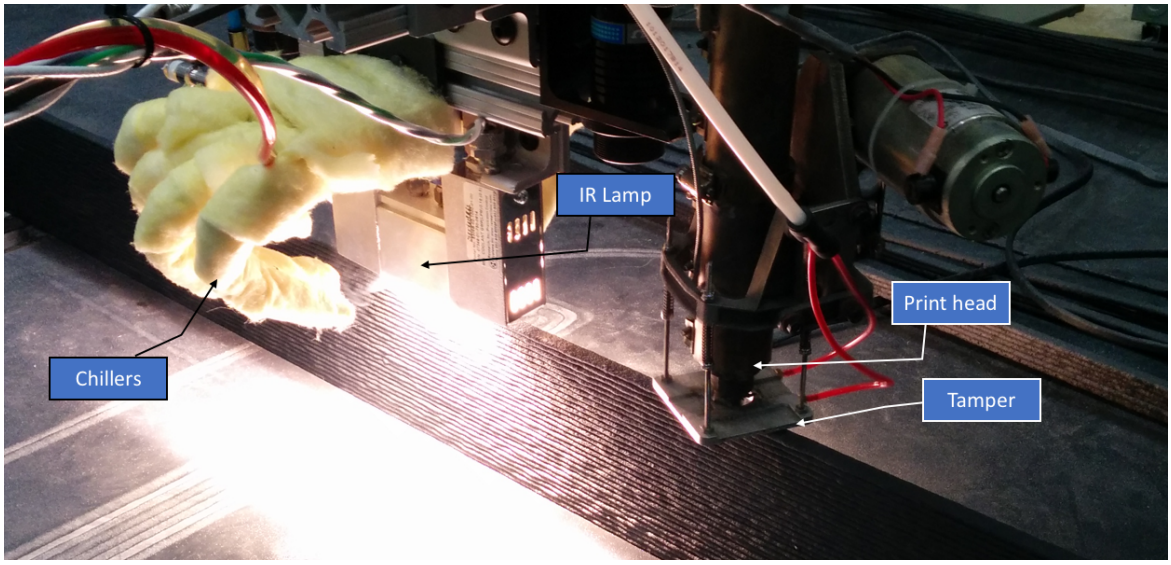

Figure 2. Deposition system during preheating.

During printing of a given layer, the underlying material (substrate) along one long side of the hexagon (the "hot side") was preheated using infrared lamps while the other side (the "cold side") was not actively heated (see Figure 1). The initial substrate temperature (T_C) was monitored by a pyrometer (Pyro-1) just in front of the heating lamp, and the pre-deposition temperature after IR preheating (T_H) was recorded by a pyrometer (Pyro-2) between the lamp and extrusion nozzle. In order to simulate longer layer times, an entire layer (both hot and cold sides) could be actively cooled by forced air chillers that were mounted adjacent to the infrared lamp. When the chillers were active during a cooling cycle, the infrared lamp was inactive and the print head moved around the hexagon without depositing material. By adjusting the number of cooling cycles between printed layers, the initial substrate temperature (T_C) could be varied between approximately 150 °C (0 cycles) and 50 °C (3 cycles). The print time for each hexagon without pausing for cooling cycles between layers was 1 h 20 min, increasing linearly with additional cooling cycles to a maximum 5 h 23 min for three cooling cycles.

Table 1 lists the initial substrate temperature (T_C) and pre-deposition substrate temperature (T_H) for each of the printed hexagons in this study. Samples on the cold side of the hexagon were deposited onto a substrate with a temperature T_C, whereas infrared lamps were used on the hot side of the hexagon to increase the substrate temperature from T_C to a pre-deposition temperature of T_H. A baseline substrate temperature of 150 °C was a control reference that represented the substrate temperature when the hexagon was printed without active heating or cooling (hexagon 4 in Table 1). The number of active cooling cycles between deposited layers was varied for hexagons 1-3 to simulate a cooler initial substrate temperature (T_C) that may occur during longer layer times when printing larger components. Infrared heating was used for hexagons 1-3 to restore the substrate temperature on the hot side (T_H) to a baseline of 150 °C just prior to deposition of new material. Hexagons 5-7 were not actively cooled, but infrared heating was used to increase the hot side substrate temperature (T_H) well beyond the baseline value of 150 °C to determine if there was an advantage of interface temperatures that approached the deposition

temperature of the material. The target substrate temperatures listed in Table 1 may vary slightly from the measured pyrometer values. Although the hot side temperature (T_H) was actively controlled by the infrared lamps and pyrometers, the cold side temperature (T_C) resulted from a discrete number of cooling cycles with the forced air chillers (hexagons 1-3) or natural cooling (hexagons 4-7).

Table 1. Target substrate temperatures for printed hexagons.

Hexagon #	# Cooling Cycles	Initial Temperature (T_C)	Pre-Deposition Temperature (T_H)
1	3	50°C	150°C
2	2	70°C	150°C
3	1	100°C	150°C
4	0	150°C	150°C
5	0	150°C	180°C
6	0	150°C	200°C
7	0	150°C	220°C

Instrumentation and Control

The printing head of the BG system was equipped with heating, cooling, and sensing elements as shown in Figure 3. The primary component for IR preheating was an infrared heating lamp (Strip IR, model number 5306B-02-1000-01-00 by Precision Control Systems). The lamp offered a high energy density per unit area (1 kW over 6.35 cm x 3.8 cm at surface level), with a maximum energy density of 41 W/cm^2. The lamp was mounted 10 mm above the printed surface to minimize heat loss and prevent accidental collisions. The heat lamp required water cooling at a minimum rate of 0.5 liters per minute, so an external cooling unit was used (Miller Coolmate 4). The lamp was connected to a Control IR 5420 control power module that allowed real-time control of the lamp power based on the pyrometer measurements.

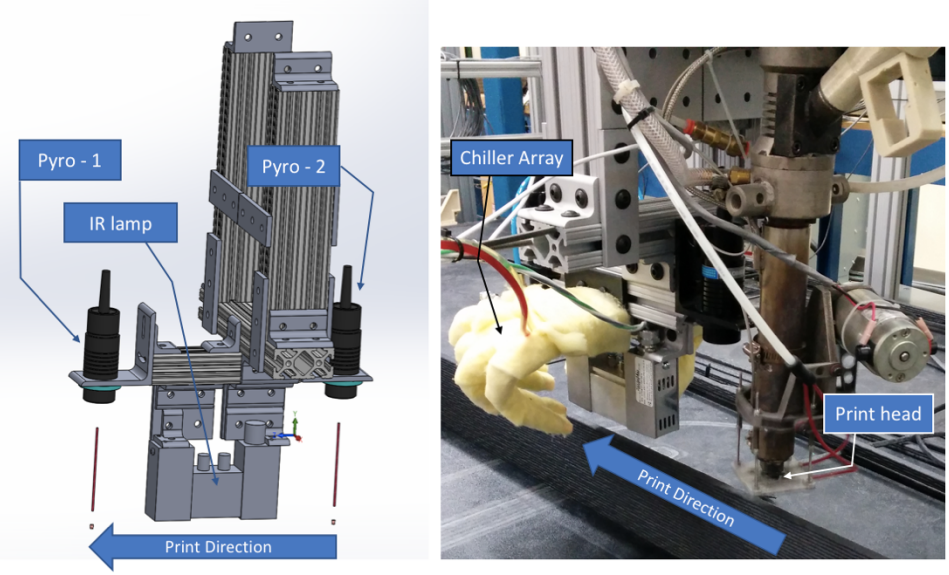

Figure 3. IR heating design (left) implemented on the BG system (right).

The pyrometers used were model number Omega OS5542A with a measurement range of -23 °C to 538 °C. The pyrometers allowed for a narrow focal diameter of 3.9 mm at a standoff distance of 150 mm. Both pyrometers were mechanically aligned and calibrated using a 95% emissivity for the material. During deposition on the hot side of the hexagon, the initial substrate temperature was recorded by Pyro-1 and the lamp power was adjusted manually to provide the desired pre-deposition temperature at Pyro-2. The maximum power required of the lamp was 85-95% of the 1kW maximum rating. Since the IR lamp was not utilized on the cold side of the hexagon and the print direction remained counter-clockwise, the pyrometers on the cold side documented the cooling rate of the just-deposited material. Data was recorded in segments at a rate of 10Hz using a National Instruments CRIO 9035 unit.

Active cooling of the printed surface was achieved by mounting an array of vortex chillers on either side of the IR heating lamp (see Figure 3). Vortex chillers are passive mechanical structures that separate a flow of compressed air at 90psi into hot and cold streams, allowing the cold stream to reach -50 °C. The chiller array was mounted such that it directed 4 jets of cold air onto the uppermost layer of the printed part from both sides of the IR lamp (total of 8 jets). The chiller manifold was insulated (yellow wrapping in Figure 3) to avoid contamination from water condensation.

Mechanical Specimens

Tensile and double-cantilever beam specimens were taken from both the hot and cold sides of each hexagon in order to correlate substrate temperature to mechanical performance. Since the orientation of the printing head remained fixed while the deposition head moved counterclockwise around the hexagon, there were transition sections (~20 cm long) at the end of the cold side and the beginning of the hot side in each layer that were not actively heated or cooled (Figure 4). These regions were excluded from analysis. The bottom 4 cm of each section was also excluded to allow for temperature stabilization from the base [27].

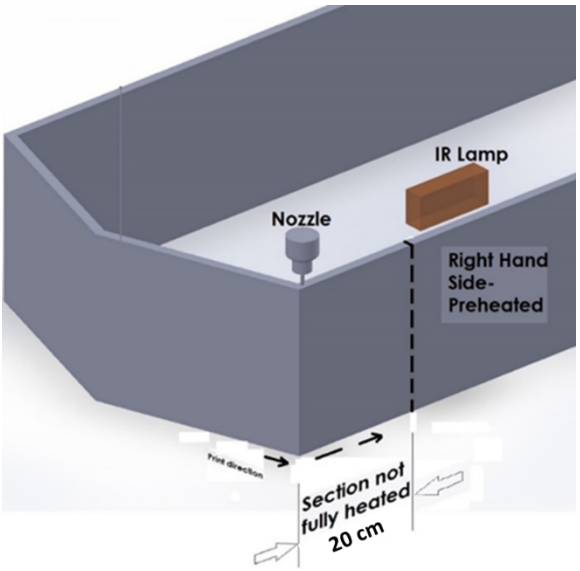

Figure 4. Sections of hexagons omitted from analysis on cold side (left) and hot side (right)

Figure 5 shows the location and numbering scheme for the mechanical test specimens from each side. The DCB samples were waterjet cut to the dimensions shown in Figure 6. The surfaces of the DCB samples were not machined (as printed) and the thickness was a single bead width (nominally 9 mm). A crack of pre-determined length (~ 25 mm) was positioned such that the crack tip was at the interface of two printed beads and the applied tensile force was perpendicular to the printed beads.

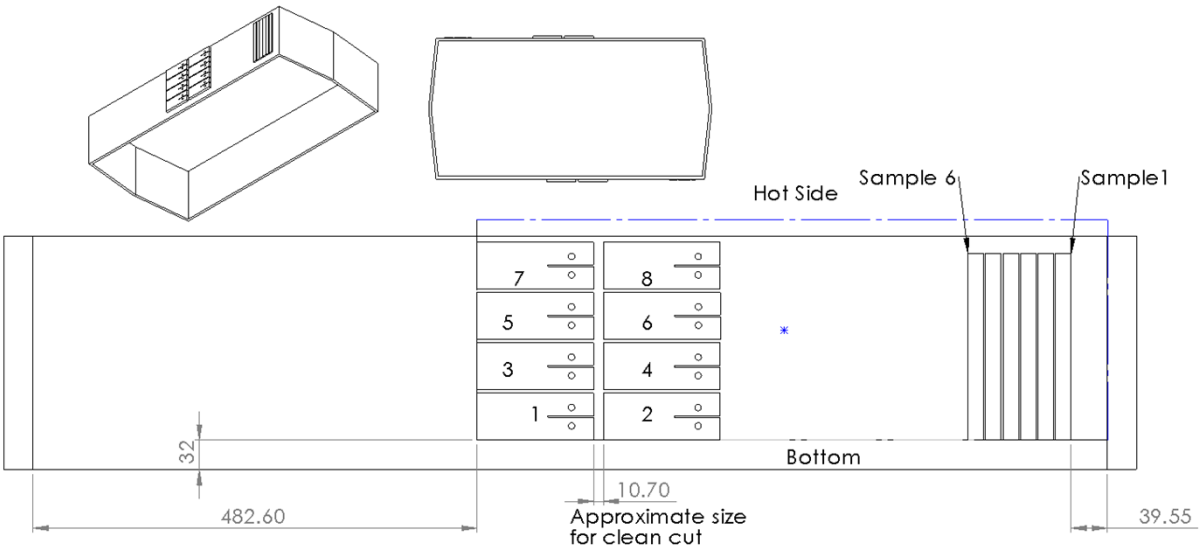

Figure 5. Location of mechanical test specimens

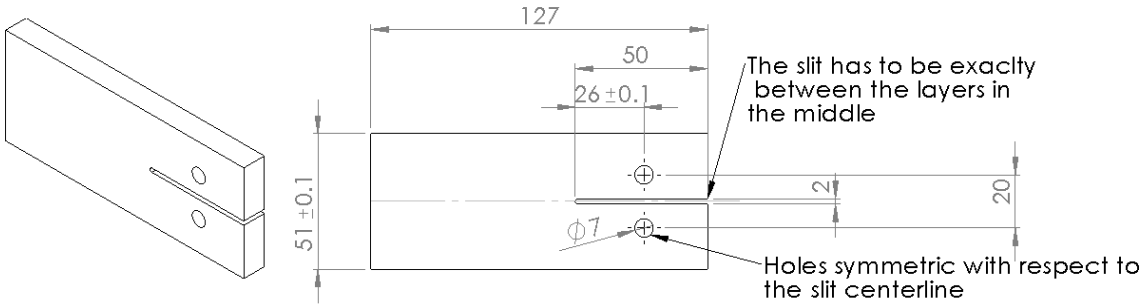

Figure 6. Double cantilever beam sample geometry. Dimensions in (mm).

Samples were dried in a vacuum oven at 50 °C for 48 hours prior to mechanical testing. The samples were tested on an MTS servo-hydraulic load frame with a 2200 N load cell and at a loading rate of 1.26 mm/min. The maximum load (P) and the corresponding displacement (δ) were recorded for each sample and the fracture energy per unit surface area was calculated according to:

$$\text{Fracture energy (kJ/m}^2\text{)} = \frac{3P\delta}{2bA_0}$$

where b is sample thickness and A_0 is the initial crack length. Eight samples were tested for each condition and the average values with standard deviations were reported.

The tensile samples shown in Figure 5 were cut from the hot and cold sections of the hexagon after the plaques were surface milled to a thickness of 6.4 mm (material removed equally from both sides). ASTM D638 type I specimens were milled from the plaques to the dimensions shown in Figure 7. Samples were stored in a desiccator at a temperature of 24° C and a relative humidity of 50 % prior to testing on an MTS servo-hydraulic load frame with a 4450 N load cell and a 200k micro-strain extensometer. Five samples for each condition were tested to failure at a rate of 1.5 mm/min and data was collected at a rate of 10 Hz.

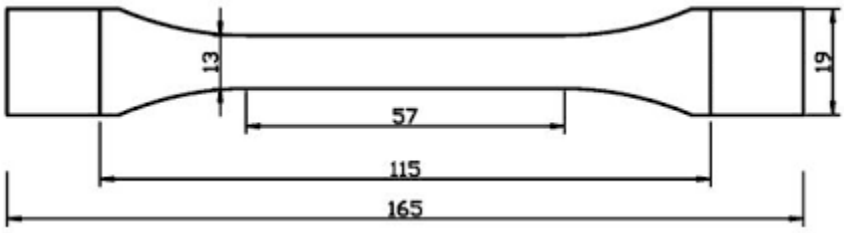

Figure 7. ASTM D638 Type I tensile specimen. Thickness = 7 mm. Dimensions in (mm).

Experimental Results

Thermal Control

The substrate temperature is plotted in Figures 8a-c for a single layer of hexagons 1-3 that were printed with active cooling cycles. The temperature of the substrate just prior to deposition of new material is shown for the hot side (T_H) of the hexagon that used infrared preheating as well as for the cold side (T_C) that did not. For example, hexagon 1 was subjected to three active cooling cycles prior to the deposition of a new layer in order to reduce the substrate temperature on both sides of the hexagon to 50 °C (T_C in Figure 8a). Infrared heating was applied only to the hot side of the hexagon during deposition of a new layer to increase the substrate temperature from a T_C of 50 °C to a T_H of 150 °C directly in front of the print head. Likewise, Figures 8b and 8c show that infrared heating was able to achieve a relatively stable preheated substrate temperature of 150 °C following active cooling of the substrate to 70 °C and 100 °C, respectively. These data show that infrared lamps are capable of preheating a substrate that was well below a material's T_g to a controlled set point temperature well above the T_g. For comparison, Figure 8d shows a relatively stable substrate temperature of 150 °C for the control case (hexagon 4) that did not receive active heating nor active cooling ($T_C = T_H$).

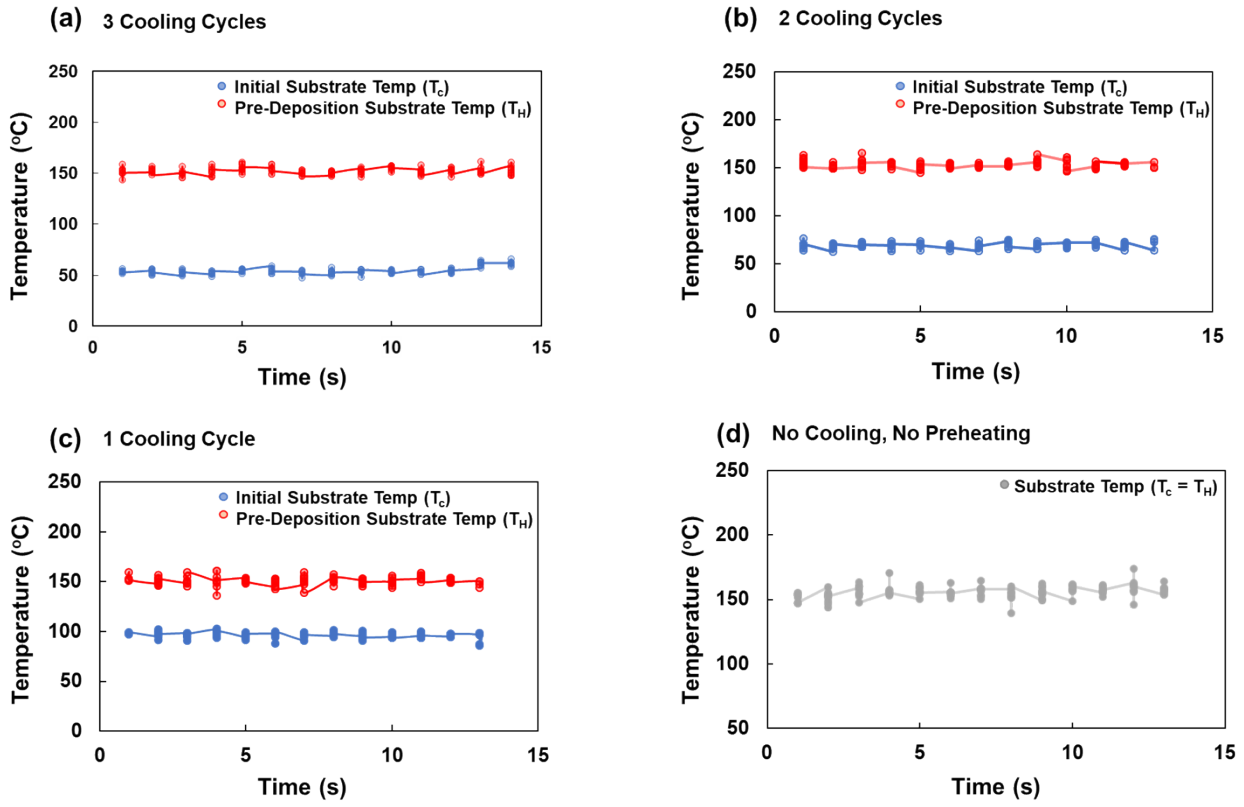

Figure 8. Temperature data for a representative substrate layer for different initial temperature (T_C) conditions. The target pre-deposition temperature (T_H) was 150 °C for each case.

The second set of hexagons did not use active cooling to achieve a desired initial substrate temperature (T_C), but instead increased the intensity of the infrared lamps to achieve higher pre-deposition temperatures (T_H = 180 °C, 200 °C, 220 °C). Since there was no pause between layers for active cooling, the initial substrate temperature (T_C) was roughly equivalent to the control case (hexagon 4) shown in Figure 9a. However, as the hot side temperature (T_H) increased for

hexagons 5-7 (Figures 9b-d), indirect heat from the infrared lamps caused a slight increase (~10 °C) in the cold side temperature (T_C) as well. For these hexagons, the initial temperature (T_C) was already above T_g and preheating was used to increase the substrate temperature (T_H) incrementally closer to the deposition temperature of 230 °C. The temperatures plotted in Figures 8 and 9 show that both T_C and T_H were stable within ± 5-10 °C of the target temperature within a given layer. The thermal history illustrated for a single layer was representative of all layers of the hexagon for a given processing condition.

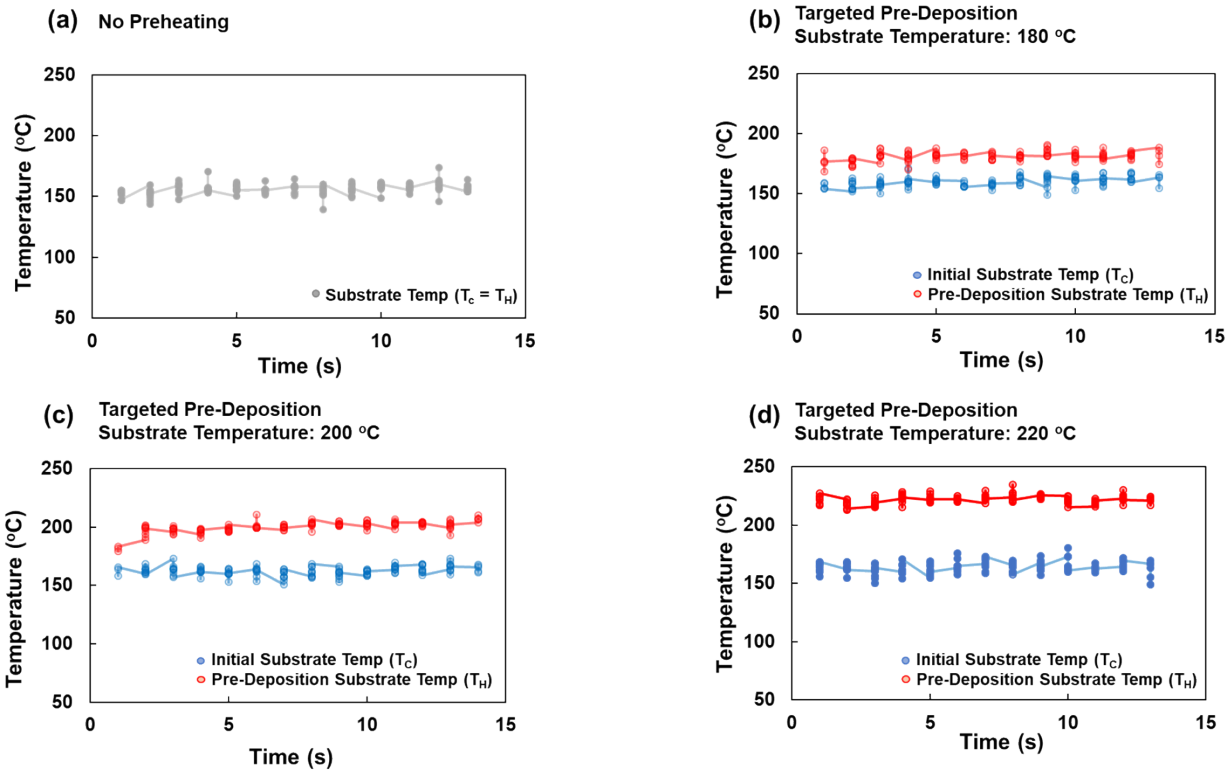

Figure 9. Temperature data for a representative substrate layer for different pre-deposition temperature conditions. The target initial substrate temperature (Tc) was 150 °C for each case.

Fracture Energy

Figure 10 compares the fracture energy of samples that were exposed to IR preheating against those that were not after each were subjected to different cooling cycles. In each case, the pre-deposition temperature (T_H) was held constant at 150 °C, including the control hexagon (#4) that did not receive any active heating or active cooling. As reflected in Table 1 and Figure 8, increasing the number of cooling cycles causes the initial substrate temperature (T_C) to decrease, which simulates longer layer times associated with larger print areas that are typical of the BAAM system. Comparing the fracture energy of samples on the cold side of the hexagons in Figure 10 (blue colums) shows that decreasing the initial substrate temperature (T_C) from a nominal value of 150 °C to 50 °C decreased the fracture energy from 5.41 kJ/m^2 to 0.63 kJ/m^2, or by a factor of ~8x. The impact of IR preheating to improve the fracture energy can be appreciated by comparing the cold side value (blue column) to the hot side value (red column)

for each sample set. Using infrared preheating to increase the substrate temperature (T_H) to a value of 150 °C caused the average fracture energy to increase significantly for all three of the actively cooled conditions (hexagons 1-3). An Analysis of Variance (ANOVA) of the fracture energy data for hexagons 1-3 showed that the improvement due to IR preheating was statistically significant with a 95% confidence level and a p-value of 0.032. For the coolest initial temperature considered here (hexagon 1), IR preheating was able to increase the average fracture energy from 0.63 kJ/m^2 to 4.23 kJ/m^2, a factor of ~7x. However, when the initial substrate temperature did not fall well below T_g (105 °C), IR preheating was not as effective. These results are similar to the previously reported observations [23-25] in which IR preheating was found to be most effective when layer times were long enough for the substrate temperature to cool well below the T_g of the material.

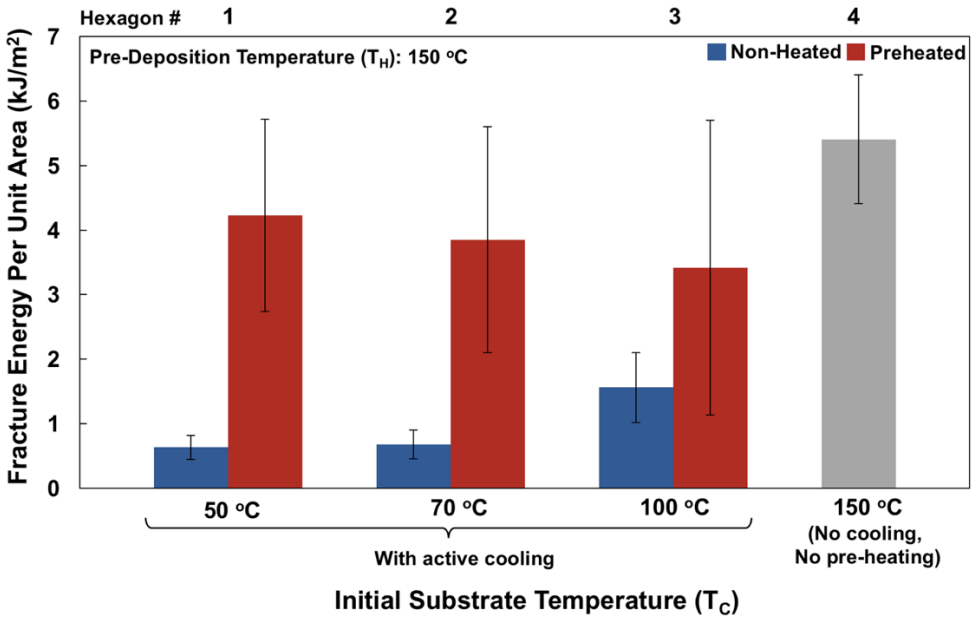

Figure 10. Fracture energy for different initial substrate temperature (T_C) conditions. Pre-deposition temperature (T_H) was 150 °C for each case.

In the second series of tests, active cooling was not used ($T_C \approx 150$ °C) and the pre-deposition substrate temperature on the hot side (T_H) was controlled by IR preheating to a range of temperatures approaching the deposition temperature of the polymer (230 °C). As shown in Figure 11, IR preheating demonstrated a 40% increase in the average fracture energy for a T_H of 200 °C, but the standard deviation of the data was too high to be statistically significant. For the preheating condition with the highest T_H (220 °C), IR preheating actually lowered the average fracture energy by ~50%, which is thought to result from local overheating of the substrate and potential polymer degradation. It is also notable that the fracture energy of the cold side increased slightly as the preheating temperature increased. Although the cold side was not directly exposed to the IR heating, it is possible that use of the lamps increased the ambient temperature of the deposition chamber and reduced the natural convective cooling of these samples (i.e. the cold side substrate temperature was slightly above the target temperature of 150 °C, see Figure 9).

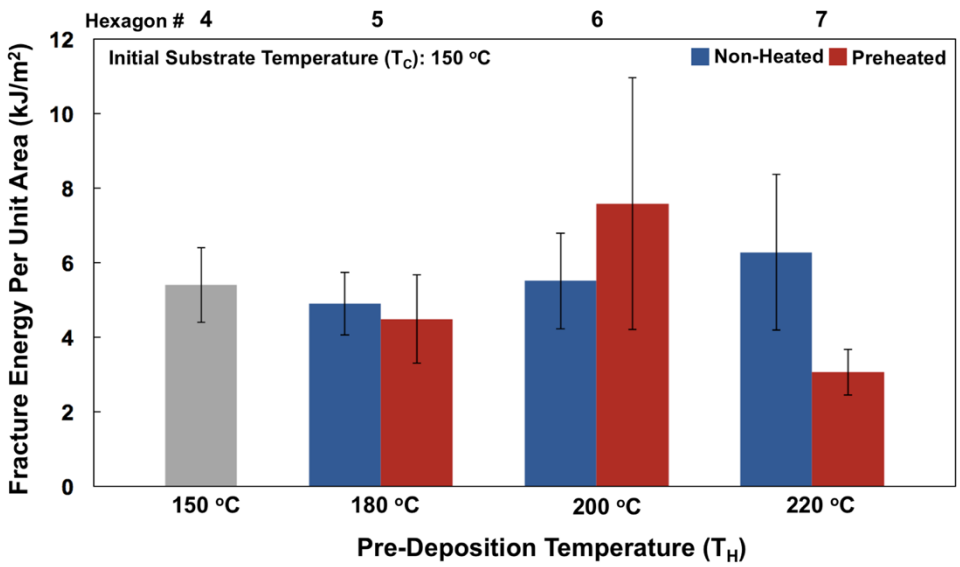

Figure 11. Fracture energy for different pre-deposition temperatures (T_H). The target initial substrate temperature (T_C) was 150 °C for each case.

Tensile Strength

The variation in the ultimate tensile strength of samples with different initial substrate temperature (T_C) is shown in Figure 12. The IR preheat temperature (T_H) for each of these samples on the hot side was held constant at approximately 150 °C. Similar to the fracture energy values in Figure 10, the z- axis tensile strength of the samples on the cold side (blue columns in Figure 12) increased significantly (135%) as the initial substrate temperature (T_C) increased from 50 °C to the refernce sample at 150 °C. Comparing the tensile strength of samples on the cold side (blue) with IR preheated samples on the hot side (red) shows a statistically significant increase due to IR preheating (ANOVA: 90% confidence, p-value = 0.097). The effect of IR preheating was most significant for the coldest initial substrate (T_C) of 50 °C, increasing from 5.1 MPa to 9.3 MPa (82%). As the initial substrate temperature (T_C) increased from 50 °C to 100 °C, the bond strength after preheating (red columns) increased slightly, but remained relatively consistent at ~10 MPa. This demonstrates the ability of IR preheating to stabilize the mechanical properties of 3D printed materials irrespective of the initial substrate temperature. Such a level of control could be especially important for large-scale printing systems that may experience long layer times and variable geometries.

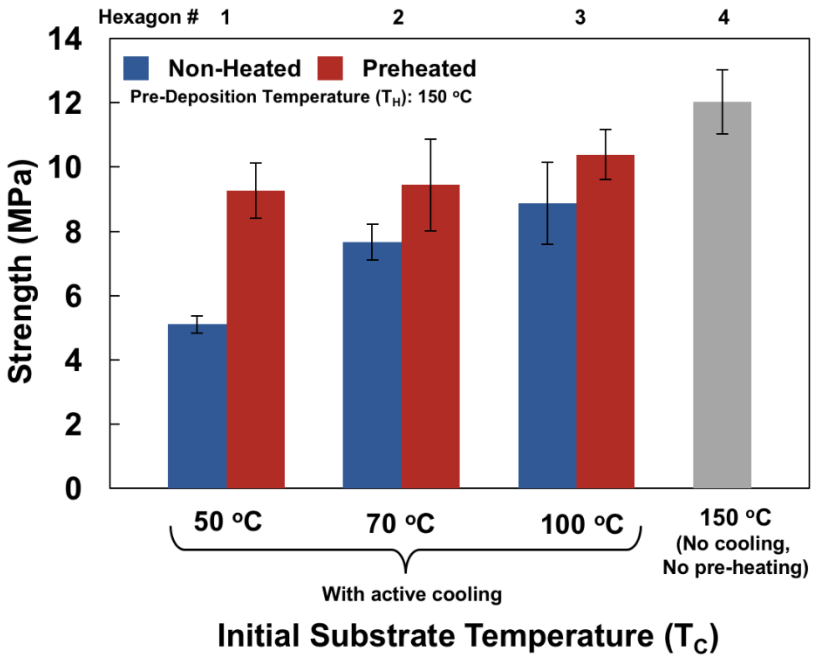

Figure 12. Ultimate tensile strength for different initial substrate temperature (T_C) conditions. Pre-deposition temperature (T_H) was 150 °C for each sample.

Figure 13 compares the fracture surface of tensile specimens from the cold and hot sides of the hexagon with an initial substrate temperature (T_C) of 50 °C. The sample that was preheated to 150 °C on the hot side showed relatively uniform failure across the polymer matrix, indicating good interdiffusion of polymer chains across the interface. By comparison, the sample that was not preheated shows poor matrix bonding and several patches of exposed carbon fibers from the surface of the bead. This indicates that when the initial substrate temperature (T_C) falls well below the T_g of the material, polymer chain mobility is inhibited and the resulting bond across the interface is weak. However, the substrate temperature can successfully be preheated well above T_g to restore mobility at the interface, encourage polymer chain entanglement, and improve the strength of the bond.

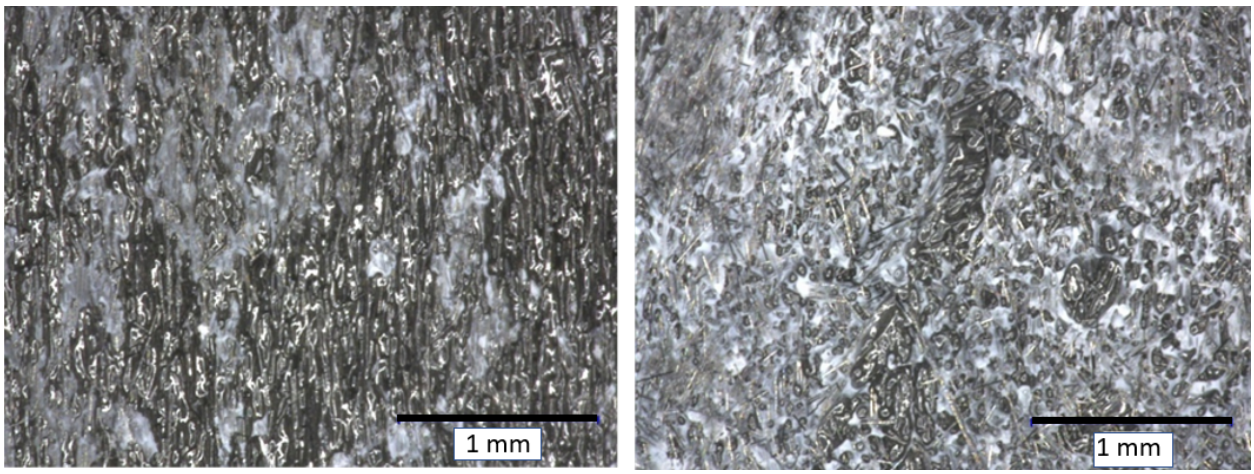

Figure 13 Fracture surface of tensile samples from the cold side (left) and hot side (right) when the initial substrate temperature (T_C) was 50 °C.

A summary of the mechanical performance for actively cooled samples in Table 2 shows that IR preheating is able to significantly improve both the fracture energy and tensile strength of the interface. However, it is notable that heating an actively cooled sample back to a surface temperature of 150 °C does not provide as good mechanical performance as the control sample that was never cooled below T_g. In other words, samples taken from the hot side of hexagons 1-3 did not perform as well as hexagon 4 that was neither actively cooled nor exposed to IR preheating. The material just below the surface of hexagon 4 was likely well above the measured surface temperature of 150 °C before deposition because it was naturally losing heat to the ambient environment. Therefore, the interface temperature following deposition of new material at 230 °C was likely around an average value of 190 °C. By contrast, the material just below the surface of the hexagon that was actively cooled to a temperature (T_C) of 50 °C was likely well below 100 °C. When IR preheating was used to increase the surface temperature of the bead (T_H) to 150 °C, there was much less thermal energy stored in the bulk of the bead. After deposition of new material, the cooler internal temperatures led to a cooler interface temperature which reduced polymer chain mobility and resulted in a slightly weaker bond. So, although IR preheating can improve the mechanical bond of a larger structure that has cooled considerably, this data shows that it would be preferable to maintain the heat within the part if possible.

Table 2. Effect of IR preheating for different initial substrate temperatures (T_C)

Hexagon #	Initial Temp (T_C)	Facture Energy (kJ/m^2)			Tensile Strength (MPa)		
		Cold	Hot	Increase	Cold	Hot	Increase
1	50°C	0.63	4.23	571%	5.1	9.3	82%
2	70°C	0.67	3.85	474%	7.7	9.4	23%
3	100°C	1.56	3.42	119%	8.9	10.4	17%
4	150°C	5.41($T_C = T_H$)		--	12.0 ($T_C = T_H$)		--

IR preheating did not have a significant impact on the tensile strength of samples for which the initial substrate temperature (T_C) did not fall well below the material's glass transition temperature (T_g). Figure 14 reports the tensile strength of samples as a function of the IR preheating temperature (T_H) with a constant initial substrate temperature (T_C) of 150 °C. Similar to the fracture energy in Figure 11, a slight increase in tensile strength was observed as the IR preheat temperature (T_H) increased up to 200 °C, but slightly decreased at 220 °C. The overall differences in tensile strength were not significant, indicating that IR preheating may not improve the interlayer bond when the initial substrate temperature (T_C) is already well above the T_g of the material, regardless of how much the substrate is heated beyond this point.

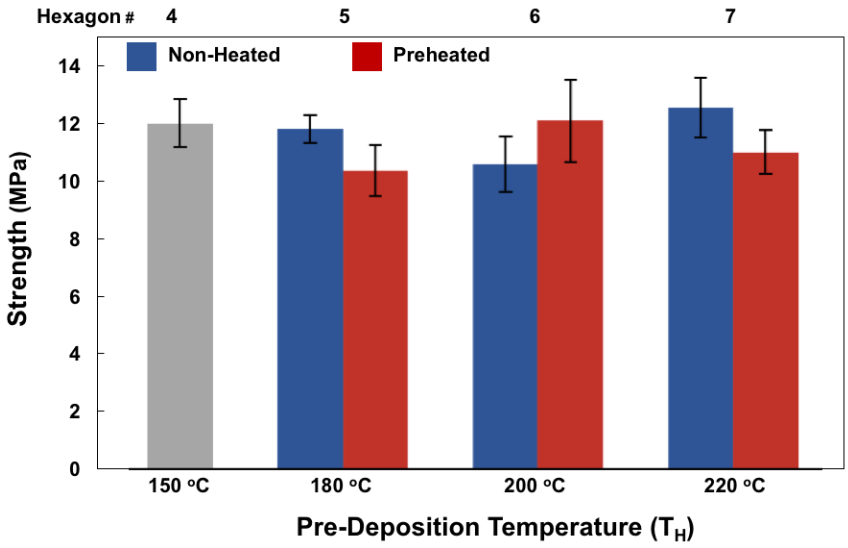

Figure 14. Ultimate tensile strength for different pre-deposition temperatures (T_H). The target initial substrate temperature (T_C) was 150 °C for each.

Conclusions and Future Work

IR preheating has been shown to be an effective means for improving the interlayer mechanical properties of 3D printed structures, especially for larger structures that have extensive layer times. This study demonstrated an experimental setup for in-situ control of the substrate temperature using an IR lamp and a pair of pyrometers mounted to the deposition head. The initial temperature of the substrate was actively cooled between deposited layers to simulate long layer times that may be encountered in large-scale printing. Regardless of the initial substrate temperature, IR preheating was able to consistently raise the pre-deposition temperature to the targeted value of 150 °C and was able to significantly improve the mechanical performance of the printed parts. For some of the cooler substrate temperatures, IR preheating was able to improve fracture energy by over 500% and tensile strength by 80%. Using IR lamps to raise the temperature of the substrate well above T_g just prior to deposition of new material is a viable means for improving polymer chain mobility across interface and strengthening the bond between printed layers. Since larger parts are also more susceptible to thermal distortion and cracking [28], the ability of IR preheating to control the bonding temperature and improve interfacial strength is especially important for these applications.

The effect of IR preheating was not significant when the substrate temperature did not drop below the glass transition temperature of the material. This is consistent with findings from other studies relating the strength of the interlayer bond to the interface temperature [18, 19]. IR preheating actually had a slightly negative impact on the bond strength at the highest settings (T_H = 220 °C), which is believed to be due to thermal degradation of the polymer during exposure to intense infrared energy. Additional studies are needed to understand and optimize the thermal transport of infrared energy within reinforced polymers that are typically used in large area additive manufacturing.

Conflict of Interest

One of the authors of this article is part of the Editorial Board of the journal. To avoid potential conflict of interest, the responsibility for the editorial and peer-review process of this article lies with a different Editor, Eric MacDonald. Furthermore, the authors of this article were removed from the peer review process and had no access to confidential information related to the editorial process for this article.

Acknowledgements

The authors acknowledge Dr. Donald Erdman at Oak Ridge National Laboratory for the use of mechanical testing facilities, Techmer ES for providing materials for this work, and Dakota Cauthen for assisting with statistical analysis. Research was sponsored by the U.S. Department of Energy, Office of Energy Efficiency and Renewable Energy, Advanced Manufacturing Office, under contract DE-AC05-00OR22725 with UT-Battelle, LLC.

References

[1] Newell, C., S. Palas, C. Duty, L. Love, V. Kunc, R. Lind, P. Lloyd, J. Rowe, R. Dehoff, and W. Peter. "Out of Bounds Additive Manufacturing." *Advanced Materials & Processes,* **171** (3) pp. 15-17 (2013).

[2] Love, L.J., C.E. Duty, B.K. Post, R.F. Lind, P.D. Lloyd, V. Kunc, W.H. Peter, and C.A. Blue. "Breaking Barriers in Polymer Additive Manufacturing." *Proceedings of SAMPE,* Baltimore, MD (2015).

[3] Ajinjeru, C., V. Kishore, P. Liu, J. Lindahl, A. Hassen, V. Kunc, B. Post, L. Love, and C. Duty. "Determination of Melt Processing Conditions for High Performance Amorphous Thermoplastics for Large Format Additive Manufacturing." *Additive Manufacturing,* **21** pp. 125-132 (2018).

[4] Kishore, V., X. Chen, C. Ajinjeru, A. Hassen, J. Lindahl, J. Failla, V. Kunc, and C. Duty. Additive Manufacturing of High Performance Semicrystalline Thermoplastics and Their Composites." *Solid Freeform Fabrication Symposium,* Austin, TX (2016).

[5] Love, L.J., V. Kunc, O. Rios, C.E. Duty, A.M. Elliott, B.K. Post, R.J. Smith, and C.A. Blue. "The Importance of Carbon Fiber to Polymer Additive Manufacturing." *Journal of Materials Research*, **29** (17) pp. 1893-1898 (2014).

[6] Curran, S., P. Chambon, R. Lind, L. Love, R. Wagner, S. Whitted, D. Smith, B. Post, R. Graves, C. Blue, J. Green, and M. Keller. "Big Area Additive Manufacturing and

Hardware-in-the-Loop for Rapid Vehicle Powertrain Prototyping: A Case Study on the Development of a 3-D-Printed Shelby Cobra" *SAE Technical Paper 2016-01-0328* (2016).

[7] Babu, S., L. Love, R. Dehoff, W. Peter, T. Watkins, and S. Pannala. "Additive Manufacturing of Materials: Opportunities and Challenges." *MRS Bulletin*, **40** (12) pp. 1154-1161 (2015).

[8] Milberg, E. "US Navy and ORNL Develop Military's First 3D-Printed Submarine Hull." *Composites Manufacturing*, online (2017).

[9] Johnson, B., L. Tryggestad, A. Obendorf, and L. Love. "3D Printed Structure Case Study: AMIE 1.0." *Proceedings of IASS Annual Symposium: Advanced Manufacturing and Materials*, Boston, MA (2018).

[10] Milberg, E. "ORNL Tool for Boeing 777x Sets World Record for Largest 3-D Printed Item." *Composites Manufacturing*, online (2016).

[11] Ahn, S.H., M. Montero, D. Odell, S. Roundy, and P.K. Wright. "Anisotropic Material Properties of Fused Deposition Modeling ABS." *Rapid Prototyping Journal*, **8** (4) pp. 248-257 (2002).

[12] Shaffer, S., K. Yang, J. Vargas, M. Di-Prima, and W. Voit. "On Reducing Anisotropy in 3D Printed Polymers Via Ionizing Radiation." *Polymer*, **55** pp. 5969-5979 (2014).

[13] Torrado-Perez, A., D. Roberson, and R. Wicker. "Fracture Surface Analysis of 3D-Printed Tensile Specimens of Novel ABS-Based Materials." *Journal of Failure Analysis and Prevention*, **14** pp. 343-353 (2014).

[14] Duty, C.E., V. Kunc, B. Compton, B. Post, D. Erdman, R. Smith, R. Lind, P. Lloyd, and L. Love "Structure and Mechanical Behavior of Big Area Additive Manufacturing (BAAM) Materials." *Rapid Prototyping Journal*, **23** (1) pp. 181-189 (2017).

[15] Sweeney, C.B., B.A. Lackey, M.J. Pospisil, T.C. Achee, V.K. Hicks, A.G. Moran, B.R. Teipel, M.A. Saed, and M.J. Green. "Welding of 3D-Printed Carbon Nanotube–Polymer Composites by Locally Induced Microwave Heating." *Science Advances*, **3** (6) (2017).

[16] Duty, C., J. Failla, S. Kim, T. Smith, J. Lindahl, and V. Kunc. "Z-Pinning Approach for 3D Printing Mechanically Isotropic Materials." *Additive Manufacturing*, **27** pp. 175-184 (2019).

[17] Compton, B., B. Post, C. Duty, L. Love, and V. Kunc. "Thermal Analysis of Additive Manufacturing of Large-Scale Polymer Composites." *Additive Manufacturing*, **17** pp. 77-86 (2017).

[18] Sun, Q., G.M. Rizvi, C.T. Bellehumeur, and P. Gu. "Effect of Processing Conditions on the Bonding Quality of FDM Polymer Filaments." *Rapid Prototyping Journal*, **14** (2) pp. 72-80 (2008).

[19] Turner, B., R. Strong, and S. Gold. "A Review of Melt Extrusion Additive Manufacturing Processes: I. Process Design and Modeling." *Rapid Prototyping Journal*, **20** (3) pp. 192-204 (2014).

[20] Partain, S. *Fused Deposition Modeling with Localized Pre-Deposition Heating Using Forced Air*, Montana State University (2007).

[21] Ravi, A. *A Study on an in-Process Laser Localized Pre-Deposition Heating Approach to Reducing FDM Part Anisotropy*, Arizona State University (2016).

[22] Ravi, A., A. Deshpande, and K. Hsu. "An in-Process Laser Localized Pre-Deposition Heating Approach to Inter-Layer Bond Strengthening in Extrusion Based Polymer Additive Manufacturing." *Journal of Manufacturing Processes*, **24** pp. 179-185 (2016).

[23] Kishore, V., C. Ajinjeru, A. Nycz, B. Post, J. Lindahl, V. Kunc, and C. Duty. "Infrared Preheating to Improve Interlayer Strength of Big Area Additive Manufacturing (BAAM) Components." *Additive Manufacturing,* **14** pp. 4-12 (2016).

[24] Kishore, V., A. Nycz, J. Lindahl, C. Duty, C. Carnal, and V. Kunc. "Effect of Infrared Preheating on the Mechanical Properties of Large Format 3D Printed Parts" *Solid Freeform Fabrication Symposium*, Austin, TX (2019).

[25] Kishore, V., C. Ajinjeru, A. Nycz, B. Post, J. Lindahl, V. Kunc, and C. Duty. "Infrared Preheating to Enhance Interlayer Strength of Components Printed on the Big Area Additive Manufacturing (BAAM) System." *SAMPE Conference Proceedings*, Long Beach, CA (2016).

[26] Roschli, A., A. Messing, M. Borish, B.K. Post, and L.J. Love. "ORNL Slicer 2: A Novel Approach for Additive Manufacturing Tool Path Planning" *Solid Freeform Fabrication Symposium*, Austin, TX (2017).

[27] Dinwiddie, R.B., V. Kunc, J.M. Lindal, B. Post, R.J. Smith, L. Love, and C.E. Duty. "Infrared Imaging of the Polymer 3D-Printing Process." *Thermosense: Thermal Infrared Applications XXXVI*, Baltimore, MD (2014).

[28] Talagani, F., S. DorMohammadi, R. Dutton, C. Godines, H. Baid, F. Abdi, V. Kunc, B. Compton, S. Simunovic, C. Duty, L. Love, B. Post, and C. Blue. "Numerical Simulation of Big Area Additive Manufacturing (3D Printing) of a Full Size Car." *SAMPE Journal,* **51** (4) pp. 27-36 (2015).